Bone 187 (2024) 117180

Contents lists available at ScienceDirect

Bone

journal homepage: www.elsevier.com/locate/bone

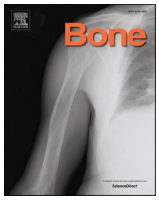

Full Length Article

The complex role of Rcor2: Regulates mesenchymal stromal cell differentiation *in vitro* but is dispensable *in vivo*

Petri Rummukainen [a,*], Kati Tarkkonen [a], Rana Al Majidi [a], Tero Puolakkainen [a], Vappu Nieminen-Pihala [a], Cristina Valensisi [b], Lauri Saastamoinen [a], David Hawkins [b], Terhi J. Heino [a], Kaisa K. Ivaska [a], Riku Kiviranta [a,c]

[a] *Institute of Biomedicine, University of Turku, Turku, Faculty of Medicine, FI-20014, Finland*
[b] *Division of Medical Genetics, Department of Medicine, University of Washington, United States of America, Division of Medical Genetics Health Sciences Building, Rm K253 Box 357720, Seattle, WA 98195-7720*
[c] *Department of Endocrinology, Turku University Hospital, PO Box 52 20521, Turku, Finland*

ARTICLE INFO

Keywords:
Osteoblast differentiation
Epigenetic regulation
Mesenchymal stromal cell

ABSTRACT

Recent research has revealed several important pathways of epigenetic regulation leading to transcriptional changes in bone cells. Rest Corepressor 2 (Rcor2) is a coregulator of Lysine-specific histone demethylase 1 (Lsd1), a demethylase linked to osteoblast activity, hematopoietic stem cell differentiation and malignancy of different neoplasms. However, the role of Rcor2 in osteoblast differentiation has not yet been examined in detail. We have previously shown that Rcor2 is highly expressed in mesenchymal stromal cells (MSC) and particularly in the osteoblastic lineage. The role of Rcor2 in osteoblastic differentiation *in vitro* was further characterized and we demonstrate here that lentiviral silencing of Rcor2 in MC3T3-E1 cells led to a decrease in osteoblast differentiation. This was indicated by decreased alkaline phosphatase and von Kossa stainings as well as by decreased expression of several osteoblast-related marker genes. RNA-sequencing of the Rcor2-downregulated MC3T3-E1 cells showed decreased repression of Rcor2 target genes, as well as significant upregulation of majority of the differentially expressed genes. While the heterozygous, global loss of Rcor2 *in vivo* did not lead to a detectable bone phenotype, conditional deletion of Rcor2 in limb-bud mesenchymal cells led to a moderate decrease in cortical bone volume. These findings were not accentuated by challenging bone formation by ovariectomy or tibial fracture. Furthermore, a global deletion of Rcor2 led to decreased white adipose tissue *in vivo* and decreased the capacity of primary cells to differentiate into adipocytes *in vitro*. The conditional deletion of Rcor2 led to decreased adiposity in fracture callus. Taken together, these results suggest that epigenetic regulation of mesenchymal stromal cell differentiation is mediated by Rcor2, which could thus play an important role in defining the MSC fate.

1. Introduction

Osteoblasts originate from mesenchymal stromal cells (MSC) that can also give rise to a number of other specialized connective tissue cell types, such as adipocytes, myoblasts and chondrocytes. Even though several molecular pathways essential for osteoblast differentiation have been described, the epigenetic mechanisms involved are still incomprehensively understood. However, the emerging literature on histone modifying enzymes, as well as DNA methylation and chromatin remodelling enzymes in the context of bone cells highlights the importance of epigenetic mechanisms in regulating bone homeostasis [1]. Histone deacetylases (Hdac1–8) have been shown to be involved in the inhibition of osteoblast differentiation, both by deacetylating histones leading to chromatin silencing and by directly regulating Runx2 activity [2–9]. In addition, several histone demethylases have been associated with osteoblast and adipocyte commitment and differentiation, including Lsd1 (Kdm1A) [10,11], Ezh2 (Kmt6) [12], Kdm6A [12], Jmjd3 (Kdm6B) [13], Jmjd2B (Kdm4B) [14] and NO66 [15].

We previously performed a genome-wide screen for transcriptomic changes during the differentiation of a mouse pre-osteoblastic cell line MC3T3-E1 [16] and identified a significant increase in the expression level of Rcor2, a close homolog of Rcor1 (also known as CoREST/

* Corresponding author.
E-mail address: pejuru@utu.fi (P. Rummukainen).

https://doi.org/10.1016/j.bone.2024.117180
Received 25 April 2024; Received in revised form 24 June 2024; Accepted 26 June 2024
Available online 27 June 2024

CoREST1). Rcor1 is an important binding partner of Lsd1 and it is required for the catalytic activity and nucleosomal substrate binding of Lsd1. Lsd1-Rcor1 complex demethylates mono- and dimethylated lysine 4 of histone 3 (H3K4), leading to transcriptional repression of closely located genes [11]. In addition, Lsd1 may act on H3K9, causing transcriptional activation in interaction with androgen receptor (AR), glucocorticoid receptor (GR) and estrogen receptor (ER) [17–20]. Lsd1-Rcor1 complex has been shown to play an important role during embryonic development and cellular differentiation of *e.g.* neuronal and hematopoietic lineages [21,22]. There are three Rcor genes in the mammalian genome. Rcors 1–3 share high structural homology with three highly preserved protein domains, including one ELM2 and two SANT domains, of which the second SANT domain is important for the binding with Lsd1 [11]. It has been experimentally demonstrated that Rcors 1–3 can all form a complex with Lsd1. Moreover, Rcors1–3 can act in an agonistic or antagonistic fashion in regulating Lsd1 activity in a context-dependent manner [23,24]. Despite important roles for Lsd1-Rcor1 complex in a variety of cell types, the functions of Rcor2 and Rcor3 are still largely unknown.

The aim of this study was to explore the dynamics and effects of Rcor2 expression on osteoblast and adipocyte differentiation *in vitro* and *in vivo*. Here, we studied the expression and role of Rcor2 in osteoblasts and adipocytes using Rcor2 silencing and RNA-sequencing. To further evaluate the importance of Rcor2 *in vivo*, we used both global knockout mice as well as conditional, limb-bud mesenchymal cell targeted knockout mice to assess the significance of Rcor2 in bone metabolism at 6 and 12 weeks of age. To study the role of Rcor2 in conditions where bone formation is challenged, we evaluated the knockout bone phenotypes in mouse ovariectomy and closed tibial fracture healing models, as well as in ageing animals at the age of 26 weeks. Our data provides novel evidence for the role of Rcor2 in osteoblast and adipocyte differentiation.

2. Materials and methods

2.1. Cell cultures

Mouse MC3T3-E1 osteoblastic cell line (CRL-2593, ATCC, USA) was maintained in αMEM medium supplemented with 10 % fetal bovine serum (FBS) and 100 U/ml penicillin-streptomycin (*i.e.*, growth medium). Osteogenic differentiation was induced by osteogenic medium (OM) composed of growth medium supplemented with 5 mM Na-β-glycerophosphate, 50 μg/ml ascorbic acid and 10 nM dexamethasone at a density dependent of the yield of cell isolation. Primary calvarial cells were isolated from calvaria of new-born mice for differentiation cultures by sequential digestions as described previously [25]. In brief, cells were isolated with five consecutive 20 min digestions with 1 % collagenase and 2 % dispase in αMEM at +37 °C and obtained fractions 2–5 were pooled and plated for culturing. After one passage, cells were plated on 6-well plates in basal growth medium at a density dependent on the yield of cell isolation. Differentiation of osteoblasts was induced at confluency by OM for 7, 14 and 21 days.

For adipocyte differentiation cultures, calvaria primary cells were cultured on 6-well plates, at a seeding density of 80 000 cells/well in growth medium. Two days post confluency, adipocyte differentiation was induced with adipocyte induction media (growth medium supplemented with 10 μg/ml insulin and 1.0 μM dexamethasone), which represents day 0 of the adipocyte culture. After two days of induction, induction media was replaced with maintenance media (growth medium supplemented with 10 μg/ml insulin). Cultures were maintained until day 11 or day 14.

Bone marrow derived osteoclast cultures [26] and rib cage derived chondrocyte cultures [27] were performed as described previously.

2.2. RNA extraction

For the RNA-seq analysis, MC3T3-E1 cells were plated in triplicates in 6-well plates at density of 100 000 cells per well. Cells were harvested at 80 % confluence representing proliferative stage, as well as at confluency and after 24 h, 14 days and 21 days of osteogenic differentiation in OM. At indicated timepoints, the cells were washed once with PBS, lysed and RNA extracted by RNeasy mini kit (Qiagen) according to the manufacturer's instructions. Quality of RNA was analyzed by Bioanalyzer, and RIN-value was measured to be >9 before sequencing. Replicate samples per each timepoint were selected for RNA-seq library preparation.

For the qPCR analysis, RNA was extracted from cell culture samples with Nucleospin RNA Plus kit (Macherey-Nagel) after homogenization in RNA lysis buffer using Ultra-Turrax T25 homogenizer (Janke&Kunkel, Germany) and eluted to 2x30μl aqua. From bone samples and tissues for the tissue panel, RNA was extracted using RNeasy Mini kit (Qiagen, USA) after pulverization of snap-frozen samples followed by homogenization in RNA lysis buffer using Ultra-Turrax T25 homogenizer.

2.3. RNA-sequencing

RNA-seq was performed on the Illumina2000 platform as 50 bp paired-end reads and processed using a standardized bioinformatic pipeline as previously described in detail [28]. Gene expression is presented in reads/kilobase pair/million mapped reads (RPKM). RNA-seq data were deposited in the Gene Expression Omnibus of the National Institute for Biotechnology Information (GSE186832).

2.4. RNA-sequencing data analysis

The raw reads were subjected to quality control using FastQC, a framework for fastq format sequencing data quality analysis. The reads were aligned to the latest version of UCSC mouse genome (mm10) using TopHat version 2.0.9 for 64bit Linux x86 [29] with default parameters that have been optimized for mammalian genomes. The data were analyzed using R version 3.0.1 for 64bit Linux x86 (http://www.r-project.org/) for Euclidean distance, Pearson correlation and Principal component analysis. Differential expression between base time point T1 and all other time points was computed in R using DESeq2 version 1.2.8 [30]. *P*-values were corrected using Benjamini-Hochberg multiple testing adjustment procedure [31].

Collective biological properties of the differentially expressed genes were investigated using pathway enrichment analysis. The pathway set used consisted of the biological process, molecular function and cellular compartment categories of Gene Ontology version 2.10.1 (http://www.geneontology.org/). Statistically enriched pathways were determined with the TopGO R toolset using the classic algorithm with Fisher statistic. The pathway enrichment analysis was repeated for each set of differentially expressed genes, generating results using each of the three Gene Ontology (GO) categories. First hierarchical agglomerative clustering was applied to the expression values of most highly time variant genes. The distance metric used in the clustering is Dynamic Time Warping (DTW), a method specifically designed to be used with time series data [32].

In order to distinguish these trends more carefully, k-means clustering was performed. To evaluate the correct number of clusters the Bayesian Information Criterion (BIC) was used to analyze the density of clustering results using different values of *k*. K-means clustering was performed using 6 clusters. Pathway enrichment analysis was performed to the clustered gene sets. Pathway enrichment using the Gene Ontology categories was computed for each gene cluster.

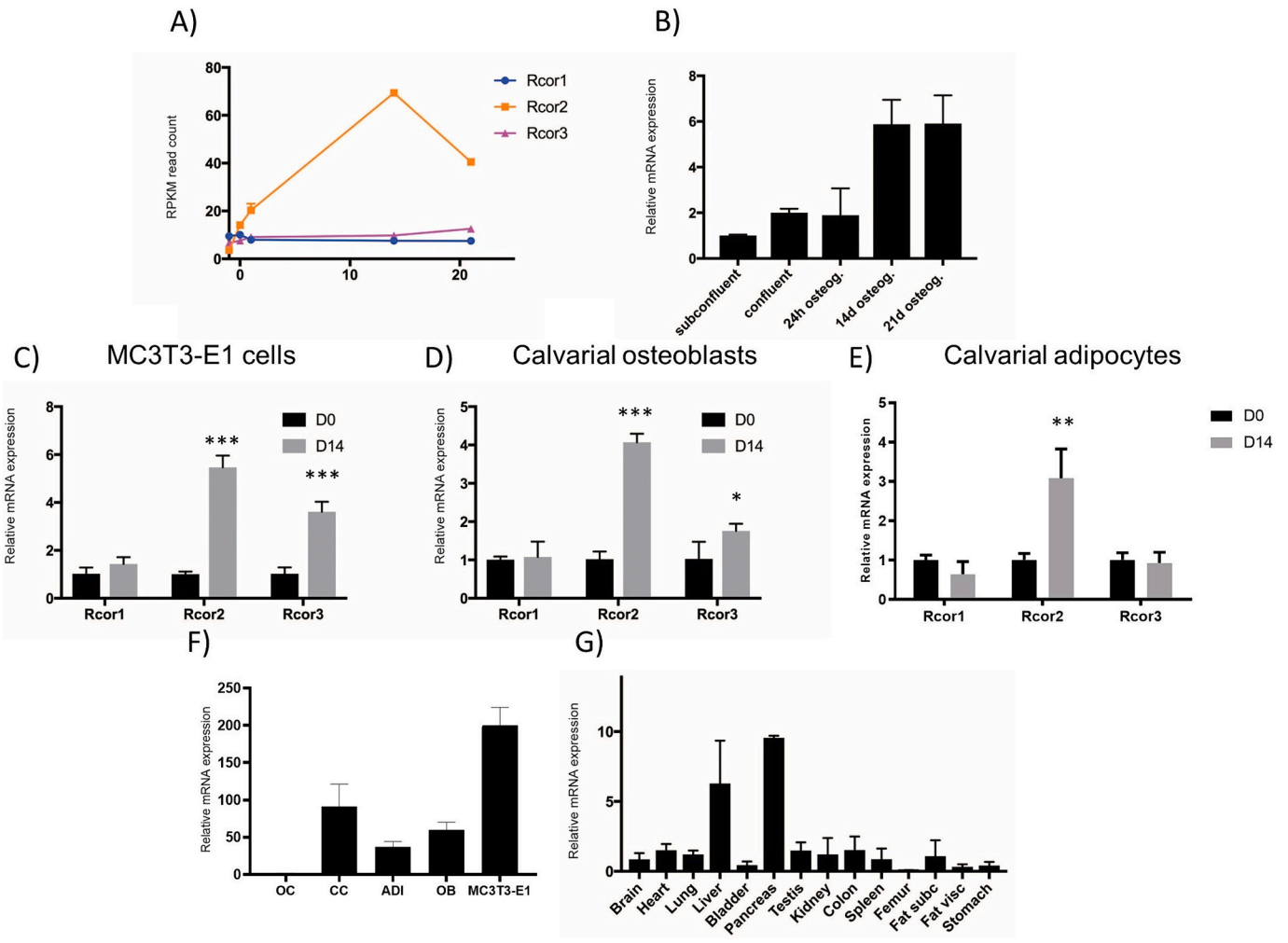

Fig. 1. Rcor2 mRNA expression profiling. A) Rcor1–3 expression presented as RPKM read count during MC3T3-E1 cell differentiation measured by RNA-seq. B) Expression of Rcor2 mRNA in mouse primary calvarial osteoblasts during differentiation measured by qPCR and normalized to the expression level of sub-confluent sample. C) Rcor1–3 mRNA expression in undifferentiated and 14d (D14) differentiated MC3T3-E1 cells measured by qPCR normalized to day 0 (D0) for each gene, D) Rcor1–3 mRNA expression in undifferentiated and 14d differentiated calvarial OBs measured by qPCR normalized to D0 for each gene, E) Rcor1–3 mRNA expression in undifferentiated and 14d differentiated calvarial adipocytes measured by qPCR normalized to D0 for each gene, F) Expression of Rcor2 mRNA in primary mouse osteoclasts (OCs), chondrocytes (CCs), adipocytes (ADI), OBs and MC3T3-E1 cells normalized to OC expression level G) Rcor2 mRNA expression in mouse tissues, $n = 3$ wildtype C57Bl mice, normalized to average expression of all samples. qPCR expression data is presented as an average + SD of three replicate cell culture wells or three replicate tissue samples. $^{*}p < 0.05$, $^{**}p < 0.01$, $^{***}p < 0.001$.

2.5. Cytochemical stainings

Cells were fixed for 15 min in 10 % phosphate-buffered formalin and stained for alkaline phosphatase (ALP) activity for 45 min at room temperature (RT) with freshly filtered ALP staining solution (0.1 mg/ml Naphtol AS MX-PO4; 0.6 mg/ml Fast Blue RR salt; 0.4 % DMF in 0.1 M Tris-HCl pH 8.3) and rinsed with water. For von Kossa staining, cells were stained with 2.5 % silver nitrate at RT for 30 min and rinsed with water. Adipocytes were washed three times with PBS and stained with freshly filtered Oil Red O (Sigma) solution for five minutes. Stained culture wells were scanned with a tabletop scanner. Representative images of the wells (three wells/culture/genotype) were analyzed with ImageJ software. Overall adipocyte area was defined by color thresholding. Percentage of the adipocyte area represents the pixel area of Oil Red O-stained adipocytes out of the total well area in pixels.

2.6. Lentiviral transduction of shRNA constructs

Lentiviral particles containing Sigma TRCII library shRNAs against Rcor2 (five constructs, TRC0000085518 - TRC0000085522, later abbreviated as 18–22) were obtained from the Functional Genomics Unit at the University of Helsinki. MC3T3-E1 were transduced by 750 µl of shRNA (p24 concentration 4.04–5.67 pg/ml), followed by selection in puromycin (3 µg/ml) for 2 days. After three passages, cells were tested to be free from viral p24 antigen and maintained in culture similarly as parental MC3T3-E1 cells. For the second RNA-seq we used MC3T3-E1-shRCOR2–18/shScrambled cells harvested at confluency, after 24 h or 7 days of osteogenic differentiation. RNA-seq data were deposited in the Gene Expression Omnibus of the National Institute for Biotechnology Information (GSE262347).

2.7. Quantitative Real-Time PCR (qRT-PCR)

RNA concentration was measured with NanoDrop One^{C} (Thermo Scientific) and the samples were stored at −80 °C. For RT-qPCR, RNA was reverse transcribed to cDNA using the SensiFast cDNA synthesis kit (Bioline, USA) with 500 ng RNA per reaction. qPCR reactions were performed using SYBR Green master mix (Thermo Scientific) with the Bio-Rad CFX96 or CFX386 Real-Time PCR Detection System and software. Ct values were normalized to beta-actin levels and $2^{-\Delta\Delta}$-Ct method

was used to analyze relative gene expression levels.

2.8. Generation of global and conditional Rcor2 knockout mouse strains

Mouse studies were approved by the Finnish Ethical Committee for experimental animals (license numbers 5186/04.10.07/2017 and 14044/2020), complying with the international guidelines on the care and use of laboratory animals and 3R principle. The animals were maintained by the skilled staff of Central Animal Laboratory (University of Turku) on a standard 12 light/12 dark cycle and fed regular soy free chow. The knockout-first (Tm1a) allele for Rcor2 gene bearing C57Bl/6NTac-Rcor2$^{tm1a(EUCOMM)Wtsi}$/Wtsieg mice (ID EM:05885) were obtained from European Mutant Mouse Archive (EMMA) (Supp. Fig. 1A). For germ line deletion of Rcor2, Tm1a-allele mice were crossed with mice expressing Cre under the control of CMV enhancer-chicken-beta-actin (CAG) promoter (CAG-Cre/2 mice) [33], creating the global knockout Rcor2KO$^{+/+}$ and Rcor2KO$^{+/-}$ mice. For conditional floxed allele generation, Tm1a-allele mice were crossed with Flp Deleter mice expressing Flp recombinase under the control of CMV enhancer and CAG promoter [34]. Mice crossed with the Flp Deleter mice were crossed with mice expressing Cre recombinase under the control of the paired related homeobox 1 promoter (Prrx1) to create the limb bud mesenchyme-specific Rcor2 conditional knockout, Rcor2$^{fl/fl}$ and Rcor2$^{-/-}_{Prrx1}$ mice. The targeted knockout was effective, leading to 70 % downregulation of Rcor2 expression as measured from marrow-evacuated femoral RNA of 6-week-old mice (Supp. Fig. 1B). There were no differences in body weight of the animals between knockout and control groups in either gender or at any time point (data not shown).

The mice were injected with demeclocyclin 2 days before sacrifice and with calcein 9 or 7 days before sacrifice for 12- and 6-week-old mice, respectively. From global and conditional knockout mice, both male and female (6–10 per group), were sacrificed at 6 and 12 weeks of age. Additionally, 10 male mice per group were sacrificed at 26 weeks of age. Tibias, femurs and inguinal adipose tissue depots were collected after CO_2-euthanasia and cervical dislocation followed by a cardiac puncture and blood collection. The bones were cleared of excess muscle and fixed overnight in 10 % formalin in PBS, followed by 70 % EtOH for at least 7 days, while adipose tissue was fixed in 10 % formalin in PBS.

2.9. Tibial fracture healing model

The closed tibial fracture procedure has been described before [35]. In brief, 10-week-old male and female mice (n = 10 per group) were anesthetized with isoflurane for 30 min after analgesia administration (buprenorphine 0.05 mg/kg and carprofen 5 mg/kg subcutaneously). A sterile stainless-steel rod (Ø 0.2 mm) was inserted to the intramedullary canal for support and a standardized, closed tibial fracture was performed using an in-house manufactured fracture apparatus [36]. Mice were treated with buprenorphine for 2 days after the procedure and sacrificed 14 or 28 days after the fracture, as described above. For µCT and histology, the tibias were carefully cleared of excess muscle to avoid damaging the calluses and fixed overnight in 10 % formalin in PBS. µCT samples were further processed by fixing in 70 % EtOH for at least 7 days.

2.10. Ovariectomy-induced bone loss

Ovariectomy (OVX) was performed on 12-week-old female mice (n = 9–10 per group) as described earlier [37]. In brief, subcutaneous injections of carprofen (5 mg/kg) and buprenorphine (0.05 mg/kg) were given and the surgical procedure was performed under isoflurane anaesthesia (250-400 ml/min 2.5 %) and aseptic conditions. A midline incision was done in the mid-dorsum of the mouse. The ovary was gently raised and removed from the surrounding fat tissue by cauterization. The ovarian horn was then released back into the peritoneum. A self-resorbing suture was placed over the muscle layer and a non-resorbing suture was set on the skin. The procedure was repeated on the contralateral side. The sham procedure was done as above except after raising the ovaries from their surroundings, they were gently put back into place and left intact. The mice were administered with post-operative injections of carprofen and monitored regularly for the next 2–3 days. Tibias and femurs were collected at 4 weeks post-operation, as described above.

2.11. Microcomputed tomography

Bones were cleaned of soft tissue and analyzed with X-ray microcomputed tomography (µCT). Cortical and trabecular bone structure of the distal femurs or proximal tibias were analyzed using µCT (SkyScan 1070, Kontich Belgium) with 8.37 µm resolution. After scanning the images were reconstructed (NRecon 1.4, SkyScan) and reoriented to ensure comparability (Dataviewer, SkyScan). The regions of interest (ROI) were drawn (CTan 1.4.4, SkyScan) on every tenth layer from 120 layers, with a total height of ~1000 µm for trabecular bone, and from 100 layers with a total height of ~840 µm for cortical bone and the results were then quantified and analyzed. The ROIs were drawn blinded for the treatment groups and quantified.

2.12. Histomorphometry

After fixation, tibias of 12-week-old male global knockout mice, were embedded in methyl methacrylate (MMA) (Sigma-Aldrich, USA). 5 µm sagittal sections were cut using a Leica RM2165 rotatory microtome and von Kossa, toluidine blue and tartrate-resistant acid phosphatase (TRACP) staining were performed on deplastified sections with standard protocols. TRACP visualizes osteoclasts as well as other myeloid cells based on their acid phosphatase activity. The slides were analyzed using Osteomeasure histomorphometry workstation (OsteomeasureXP 3.1.0.1, Osteometrics, USA). The analyzed area of the tibias was defined as 1.30 mm^2 × 0.84 mm^2, starting 200 µm distally from the growth plate, excluding the cortical border areas with a 100 µm margin. Static parameters were measured from toluidine blue and TRACP stained slides and dynamic parameters from unstained slides according to standardized protocols [38].

2.13. Adiposity in callus area

For histological analyses, tibias from the fracture experiment were fixed in 3.7 % formalin, decalcified in 10 % EDTA, embedded in paraffin, and cut into 4 µm sections. Sections were deparaffinized, rehydrated, and stained with haematoxylin and eosin (H&E) using standard procedures. Samples were scanned with 3DHISTEC PANNORAMIC 1000 slide scanner. Number of adipocyte 'ghosts' was counted manually from the fracture callus area in tibial sections using 3DHISTEC CaseViewer programme. Area was standardized to 23 mm^2 in all samples, covering the entire callus area. Number of adipocyte 'ghosts' was normalized to the area and reported as adipocyte number/mm^2.

2.14. Biomechanical testing

Samples for biomechanical testing were carefully cleared of muscles to avoid damaging the calluses and stored in −20 °C wrapped in PBS-soaked gauzes to avoid dehydration. Biomechanical testing was performed with a compression device (Lloyd Instruments, Fareham, UK) with a calibrated 100 N load cell. The samples were subjected to a three-point bending test, where the tibia was placed on a two-point sample holder 10 mm apart. Load was applied to the middle of the callus with the rate of 1 mm/min until fracture occurred. Stiffness, maximum load, post-yield displacement and amount of work-to-fracture were analyzed using Nexygen (v.4.7 issue 10, Lloyd instrument Ltd., Fareham, UK). The reported outcome parameters are illustrated in Supplemental Fig. 1C.

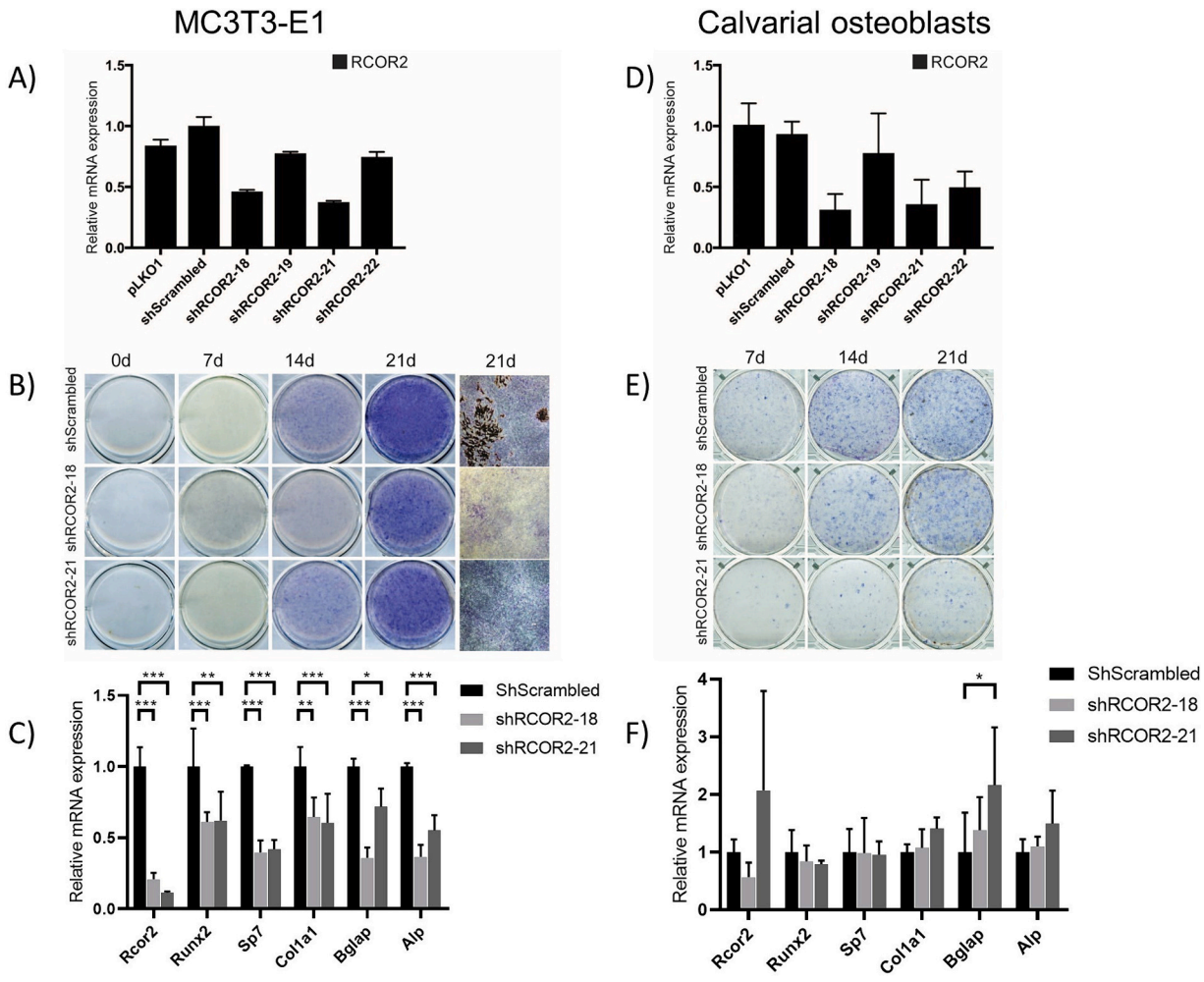

Fig. 2. A) Silencing of RCOR2 mRNA expression in MC3T3-E1 cells by shRNA expression. B) ALP and Von Kossa staining of differentiation culture of shRCOR2–18 and shRCOR2–21 expressing MC3T3-E1 cells. C) qPCR analysis of Rcor2, Runx2, Sp7, Col1a1, Bglap and Alp mRNA expression in shRCOR2–18 and shRCOR2–21 MC3T3-E1 cells after 14 days of differentiation, normalized to shScrambled. D) shRNA silencing of Rcor2 mRNA expression in mouse primary calvarial osteoblasts, E) ALP staining of differentiation culture of shRCOR2–18 and shRCOR2–21 expressing mouse primary calvarial osteoblasts F) qPCR analysis of Rcor2, Runx2, Sp7, Col1a1, Bglap and Alp mRNA expression in shRCOR2–18 and shRCOR2–21 expressing mouse primary calvarial osteoblasts cells after 14 days of differentiation, normalized to shScrambled. $*p < 0.05$, $**p < 0.01$, $***p < 0.001$.

2.15. Statistical analysis

Results are presented as mean with standard deviation (SD). The results were tested for normal distribution with the Shapiro-Wilk normality test and outliers with the ROUT method with Q = 1 %. Changes between groups were analyzed using Student's two-tailed *t*-test, one-way ANOVA or Kruskall-Wallis test using Bonferroni's multiple comparison correction where applicable, with the GraphPad Prism 8.3.0 software. Statistical significance was set to $p < 0.05$.

3. Results

3.1. Dynamic changes in Rcor2 mRNA expression during in vitro osteoblast and adipocyte differentiation

We have previously performed a whole transcriptome RNA-seq analysis of differentiating mouse MC3T3-E1 cells, including cells at proliferative stage and at confluency, as well as cells differentiated for 24 h, 14 days or 21 days in OM [16]. Rcor2 was identified among the most significantly upregulated genes during osteoblast differentiation. When compared to proliferating cells, Rcor2 showed 3-fold upregulation at the confluent state, 5-fold upregulation after 24 h of osteogenic induction, and 10-fold upregulation in the cells differentiated for 14 days, as well as mature osteoblasts on day 21. Rcor2 homologues Rcor1 and Rcor3 did not show any significant dynamics in the RNA-seq analysis, although they were expressed in MC3T3-E1 cells (Fig. 1A). To verify this finding, Rcor2 mRNA level was measured by qPCR in mouse primary calvarial osteoblasts at the same culture conditions and timepoints that were used for MC3T3-E1 RNA-seq analysis and a very similar expression pattern was found, indicating upregulation of Rcor2 during osteoblast differentiation (Fig. 1B). Moreover, when mRNA levels of Rcors 1–3 were measured by qPCR in both MC3T3-E1 and primary calvarial osteoblasts, Rcor2 was found to be the most upregulated of all three Rcors with a 5.9-fold and 4.3-fold upregulation at 14 days ($p < 0.001$ for both) (Fig. 1C, D). Rcor3 was also upregulated in MC3T3-E1 cells (3.9-fold, $p < 0.001$) and in primary osteoblasts (1.8-fold, $p = 0.020$) differentiated for 14 days when compared to undifferentiated cells (Fig. 1C, D). When analyzed in calvarial adipocytes, differentiated for 14 days, Rcor2 was the only Rcor with a significantly increased expression level (3-fold, $p = 0.009$) (Fig. 1E). Next, Rcor2 mRNA expression was measured in mouse bone marrow derived primary osteoclasts, rib cage derived chondrocytes and calvaria derived cultured adipocytes and the expression level was compared to primary osteoblasts and MC3T3-E1 cells (Fig. 1F). Rcor2 mRNA was found to be expressed in all mesenchymal lineage cells, including osteoblasts, chondrocytes and adipocytes, whereas osteoclasts derived from hematopoietic lineage showed no detectable

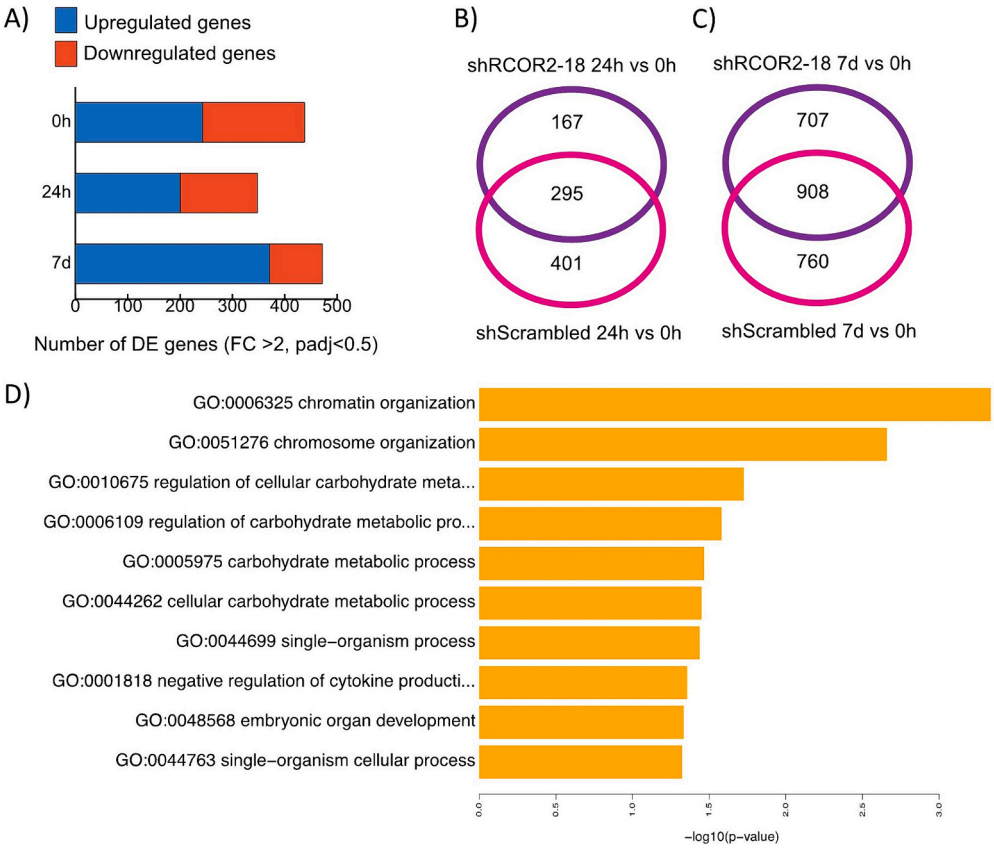

Fig. 3. shRCOR2 RNA-seq data. A) Number of DE genes in shRCOR2–18 compared to shScrambled MC3T3-E1 cells at 0, 24 h and 7d after osteogenic induction. B, C) Number of common and unique >2-fold DE genes in shRCOR2–18 and shScramble cells in cells differentiated for 24 h (B) and 7d (C) compared to 0 h cells. D) Top GO terms from DE genes.

Rcor2 expression. In a tissue panel of 14 mouse tissues collected from a wild-type C57Bl mouse, high Rcor2 mRNA expression was found in liver and pancreas but signal was detected also in many other organs, suggesting a relatively low but ubiquitous expression of Rcor2 mRNA in mouse tissues (Fig. 1G). Interestingly, Rcor2 expression in the femur sample was very low compared to other tissues, which was probably due to the presence of bone marrow, thus masking the overall expression of Rcor2 in bone.

3.2. *Rcor2 silencing leads to impaired differentiation of MC3T3-E1 and primary calvarial osteoblasts*

To study the relevance of Rcor2 upregulation during osteoblast differentiation, Rcor2 expression was silenced in MC3T3-E1 cells by stable shRNA expression. Approximately 50 % downregulation of Rcor2 mRNA was obtained in two pools of shRNA expressing cells (constructs 18 and 21) and 10 % downregulation in two different pools (constructs 19 and 22) (Fig. 2A). When performing a differentiation culture of the two selected cell pools (shRCOR2–18 and shRCOR2–21), which showed most downregulation of Rcor2, less ALP-positive cells were found at 14 and 21 days of differentiation, and more importantly no visible bone nodules were seen in von Kossa staining at 21 days when compared to the shScrambled control cells (Fig. 2B). Furthermore, the expression of osteoblast related genes in shRCOR2–18 and shRCOR2–21 silenced cells was studied during osteogenic differentiation and significantly decreased mRNA levels of *Runx2* ($p < 0.001$ and $p = 0.001$), Osterix (*Sp7*) ($p < 0.001$ and $p < 0.001$), Collagen type I alpha 1 chain (*Col1A1*) ($p = 0.002$ and $p < 0.001$), Osteocalcin (*Bglap*) ($p < 0.001$ and $p = 0.015$) and ALP (*Alp*) ($p < 0.001$ and $p < 0.001$) were detected in shRCOR2–18 and shRCOR2–21 cells, respectively, suggesting impaired osteoblastic differentiation (Fig. 2C). Rcor2 silencing did not affect MC3T3-E1 cell proliferation (data not shown). The effect of shRNA mediated Rcor2 silencing was also partly recapitulated on the differentiation of mouse primary calvarial osteoblasts, as evaluated by ALP-positive cells (Fig. 2D, E), although mRNA expression data did not support the observed difference in osteoblastic differentiation (Fig. 2F).

3.3. *Rcor2 knockdown mitigates the repression of target genes and supports proliferation of MC3T3-E1 osteoblasts*

To identify target genes and mechanisms of action of Rcor2 in osteoblasts, RNA-seq analysis was performed on the knockdown cell line with the construct demonstrating highest downregulation of Rcor2 (shRCOR2–18) and on the control cells (shScramble) at confluency and after 24 h or 7 days of osteogenic stimulation. These timepoints represent the onset and early phases of differentiation, when Rcor2 mRNA expression was strongly upregulated in OM in parental MC3T3-E1 cells (Fig. 1A). When comparing shRCOR2–18 cells to shScrambled cells at 0, 24 h and 7 days, 438, 348 and 472 genes that were >2-fold significantly differentially expressed (DE) were found at each time point, respectively (Fig. 3A). In general, there were more upregulated than downregulated genes in shRCOR2–18 cells expressing less Rcor2, supporting the previous observations that Rcor2 acts in a transcriptional repressor complex [39]. When examining the gene expression changes during the first 24 h of differentiation (24 h), there were close to 700 DE genes in the control cells, but only 462 in shRCOR2–18 cells when compared to 0 h. From these DE genes 295 were common for both cell pools, thus there were more uniquely behaving genes in the control cells than in Rcor2 knockdown cells (Fig. 3B). In turn, in the cells differentiated for 7 days *vs.* cells at confluency (0 h), there were similar numbers of DE genes in the control (1668) and shRCOR2–18 (1615) cells, of which 908 were overlapping between the cell types (Fig. 3C). The differences in the

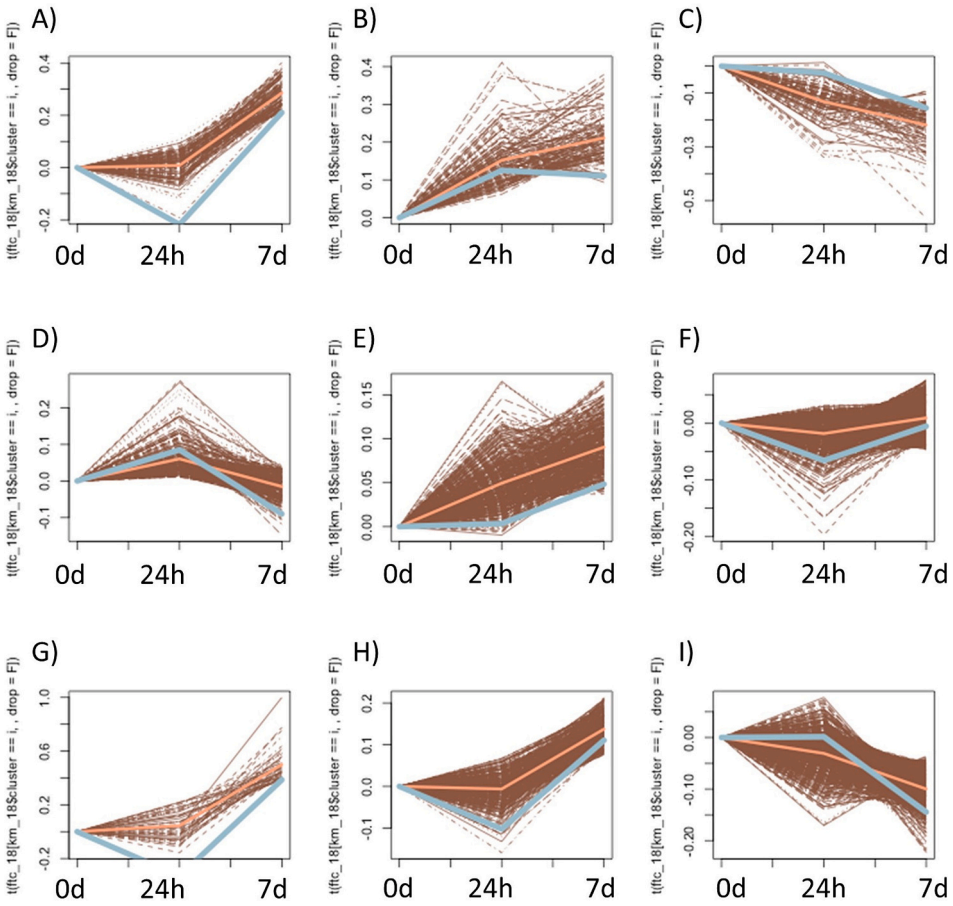

Fig. 4. K-means clustering of DE genes between shRCOR2–18 and shScrambled cells. Orange line represents the average expression level of genes in shRCOR2–18 cells in each cluster. Grey line represents average expression level of the same genes in ShScrambled control cells.

Table 1
Log2 fold change of the top 15 most significantly Differentially Expressed (DE) genes in shRCOR2 cells compared to shScrambled cells at each timepoint.

Gene name	Log2 FC 0 h	Gene name	Log2 FC 24 h	Gene name	Log2 FC 7d
Ptx3	2.7	Sfrp2	1.8	Serpine2	1.5
Spp1	−2.2	Cbr2	−1.6	Ddx3y	2.6
Col2a1	2.3	Col2a1	1.7	Sfrp2	1.7
Npr3	2.4	Cpe	−1.2	Wisp2	2.0
Sparcl1	−1.7	Spp1	−1.2	1500015O10Rik	2.3
Tnn	1.9	Tnfrsf11b	−1.7	Itgbl1	2.2
Gpnmb	−2.8	Sparcl1	−1.2	Mgat4b	1.4
Cyp26b1	2.3	Tnn	1.4	Fndc1	3.5
Spon2	−2.5	Sorbs1	−1.6	Lum	1.6
Sfrp2	1.5	Ptx3	1.5	Apod	2.3
Cxcl12	1.9	Dmpk	−2.0	Pcolce	1.1
Serpine1	1.7	Gm16332	−1.4	Adamts2	1.6
Slc1a3	1.6	Scara5	−1.0	Kdm5d	2.3
Dmp1	−2.2	Cfh	−1.4	Uty	2.5
Nov	−1.4	Chrdl1	−1.2	Adgrg6	1.6

number of DE genes between the samples indicate that there were more transcriptional changes induced by osteogenic medium in the control cells at the onset of differentiation, suggesting a delayed response to osteogenic stimulus in the Rcor2 knockdown cells. Top 15 of significantly DE genes in each timepoint are presented in Table 1 and complete tables are included as Supplementary material (Table S1). The top GO terms of DE genes include chromatin and chromosome organization as well as metabolic processes (Fig. 3D).

The DE genes were then subjected to K-means clustering to find similarly behaving gene clusters over time. To reveal potentially significant patterns, nine clusters were generated from genes showing DE expression in any of the measured samples (Fig. 4A-I). GO pathway analysis results from the biological process (BP) category for each cluster are presented in Supplementary information (Table S2). The average expression level of genes in each cluster (represented by an orange line for shRCOR2–18 and a grey line for the shScramble) had more variability in the curves at 24 h timepoint than at 7 days. This might indicate that induction of Rcor2 is important specifically in a rapid response to osteogenic stimulation, for example in repressing genes that potentially maintain cells in a proliferative stage. We then evaluated individual gene clusters (Fig. 4A-I). Cluster D showed upregulation at 24 h and repression at 7 days in both cell types, suggesting that these genes respond rapidly to osteogenic medium (Fig. 4D). Pathway enrichment analysis revealed this cluster to contain *e.g.* interferon signalling related pathways, which could be related to the known connection between interferon signalling and glucocorticoids [40] and the presence of dexamethasone in the osteogenic medium.

Two clusters (Fig. 4C, I) showed downregulation over time in both shRCOR2–18 and control cells, with minor differences in their average expression profiles. Genes in these clusters were strongly associated with pathways regulating cell cycle, migration and cell motility, and could thus be regulated rather by cell confluence than by direct consequences of Rcor2 expression levels, and they were not considered as candidates for further studies. Based on these general observations and on the fact that Rcor2 is a known component in a repressor complex, we chose three clusters (Fig. 4A, E and H) showing strongest upregulation in shRCOR2–18 cells to a more detailed analysis.

BP terms enriched in cluster A (Fig. 4A) were strongly associated with nucleotide biosynthesis and metabolic processes, which might refer

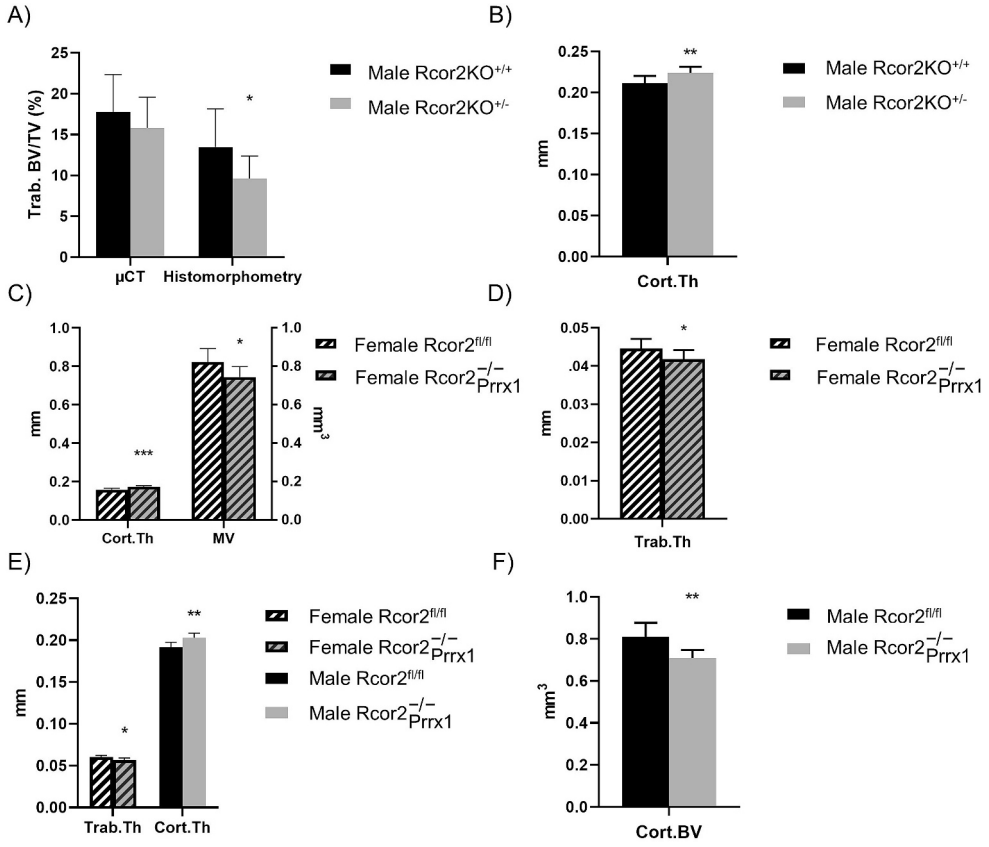

Fig. 5. Bone phenotype of Rcor2 knockout mice. A) Trabecular BV/TV was decreased slightly in μCT and significantly in histomorphometric analyses of 12-week-old male Rcor2KO$^{+/-}$ mice femurs compared to controls. B) Cortical thickness of 12-week-old male Rcor2KO$^{+/-}$ mice tibias was significantly thicker than control mice. C) Cortical thickness of 6-week-old female Rcor2$^{-/-}_{Prrx1}$ mice femurs was significantly increased compared to control mice, resulting in a smaller marrow volume. D) Trabecular thickness of 6-week-old female Rcor2$^{-/-}_{Prrx1}$ mice tibias was decreased compared to controls. E) Trabecular thickness of tibias of 12-week-old females was decreased compared to controls, and males had increased cortical thickness in femurs compared to controls. F) Cortical bone volume of 26-week-old male Rcor2$^{-/-}_{Prrx1}$ mice femurs was decreased compared to controls. * $p < 0.05$, **$p < 0.01$.

to attenuation of DNA replication and cell proliferation in the control cells when differentiation is induced, thus suggesting that shRCOR2–18 cells maintain proliferative state longer than the control cells. Interestingly, genes related to Tgf-β signalling pathway, which is known for the recruitment of mesenchymal stem cells to the bone resorption pit during bone remodelling cycle, were enriched in cluster A.

In cluster E (Fig. 4E), which represent upregulated genes in Rcor2 knockdown cells at both at 24 h and 7-day time points, enriched BP terms were associated with *e.g.*, amino acid metabolic processes, skeletal and limb morphogenesis, mesenchymal cell proliferation and neuronal differentiation. In cluster H (Fig. 4H), GO-terms were associated with chromosomal organization. However, the average expression profiles of many of the upregulated DE genes increased at 7-day time point also in the control cells, indicating the importance of these genes in the differentiation process. Whether their stronger upregulation in Rcor2 knockdown cells results from the direct effects of Rcor2 action or some feedback mechanisms related to impaired onset of cell differentiation, remains open.

3.4. *In vivo bone phenotype of Rcor2 deletion is less prominent*

To study the role of Rcor2 *in vivo*, a global Rcor2 knockout mouse strain (Rcor2KO) was generated by using knockout-first allele carrying mice (Supp. Fig. 1A). The homozygous mice with the Tm1a knockout-first allele containing the LacZ-Neo insertion cassette upstream of the Rcor2 gene were viable and fertile. However, after deletion of the Neo cassette together with the 7 first exons of the Rcor2 gene, homozygous Rcor2KO$^{-/-}$ embryos were lost *in utero* before E8.5. Due to the scope of this study in postnatal bone growth and homeostasis, the exact developmental phase of Rcor2KO$^{-/-}$ lethality was not determined, but it is evident that Rcor2 is required for the early embryonal development, which is consistent with previous reports [39,41]. These results are an example of a situation where the insertion cassette upstream of the gene of interest is not sufficient to disturb the gene transcription and thus, the knockout-first allele may result in either wildtype or in hypomorph mice regarding their gene expression status.

Despite the fatal effect of homozygous Rcor2 deletion, the heterozygous Rcor2KO$^{+/-}$ were viable, fertile and indistinguishable from the wildtype littermates. To study possible changes in bone homeostasis, the bone phenotype of femurs from 6-week-old and tibias of 12-week-old Rcor2KO$^{+/-}$ and Rcor2KO$^{+/+}$ male and female mice was analyzed by μCT. There were no detectable major differences in trabecular or cortical bone compartments, including measures of trabecular bone volume / tissue volume ratio (BV/TV) (Fig. 5A), trabecular number (Tb.N.), trabecular thickness (Tb.Th.), separation (Tb.S.) or cortical bone mineral density (BMD) or bone volume (Cort. BV) (Supp. Table S3), although cortical thickness was significantly increased ($p = 0.008$) in tibias of 12-week-old male mice ($n = 8$–9/group) (Fig. 5B). On the other hand, there was a 30 % decrease in trabecular BV/TV in histomorphometry analysis of Rcor2KO$^{+/-}$ male mice tibias ($n = 6$/group) (Fig. 5A).

To study the effect of homozygous Rcor2 deletion in bone, Rcor2 deletion was targeted to long bone mesenchymal progenitor cells by using Prrx1-Cre mouse strain (Supp. Fig. 1A). Resulting Rcor2$^{-/-}_{Prrx1}$ mice

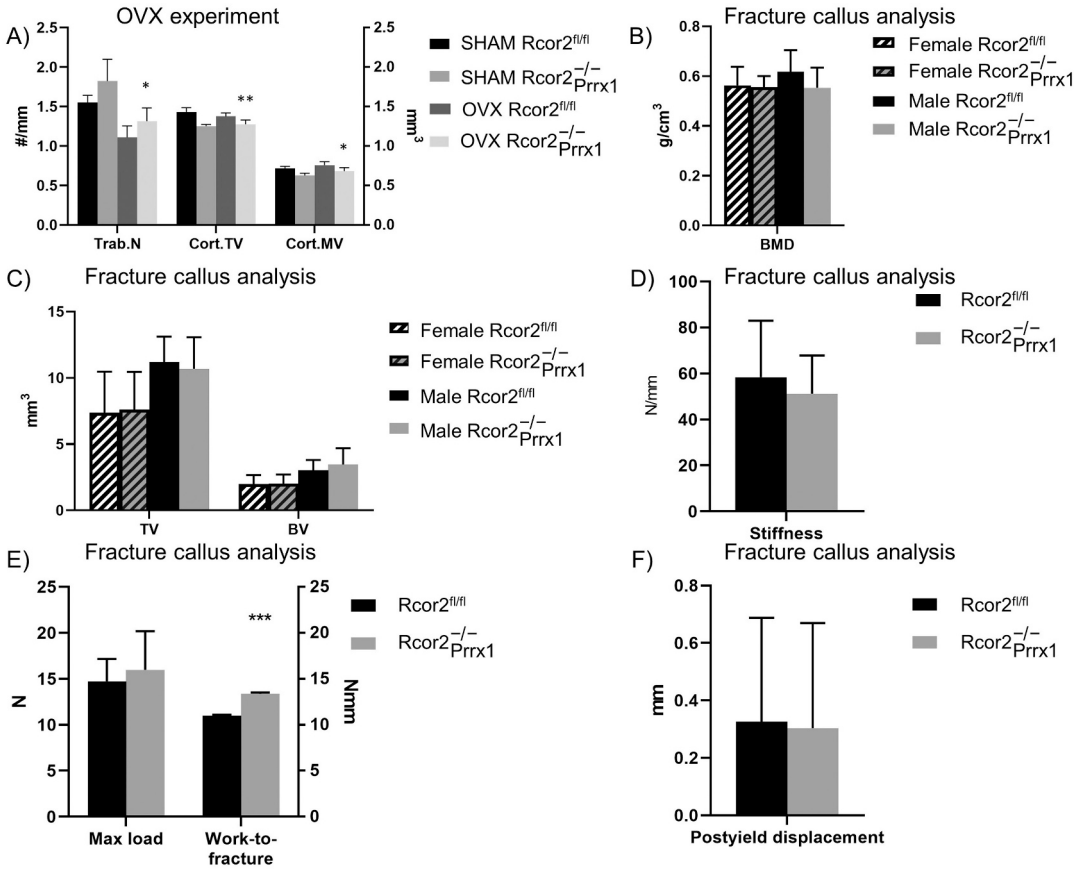

Fig. 6. Rcor2$^{-/-}_{Prrx1}$ mice do not have a more severe phenotype after OVX or fracture healing. A) Rcor2$^{-/-}_{Prrx1}$ OVX mice had increased number or trabeculae, decreased cortical tissue and marrow volumes in femurs compared to controls. B) Fracture callus BMD of Rcor2$^{-/-}_{Prrx1}$ mice was unchanged compared to controls. C) Fracture callus tissue and bone volumes of Rcor2$^{-/-}_{Prrx1}$ were unchanged compared to controls. D) 3-point-bending of fracture calluses of Rcor2$^{-/-}_{Prrx1}$ mice showed no differences compared to control mice. E) Maximum load of Rcor2$^{-/-}_{Prrx1}$ fracture calluses was comparable to controls, but work-to-fracture was significantly increased in the Rcor2$^{-/-}_{Prrx1}$ group. F) Post-yield displacement of Rcor2$^{-/-}_{Prrx1}$ mice fracture calluses was unchanged compared to control mice. *$p < 0.05$, **$p < 0.01$, ***$p < 0.001$.

had no phenotype in terms of body weight, general well-being or fertility. The bone phenotype of Rcor2$^{-/-}_{Prrx1}$ mice was studied by μCT at 6, 12 and 26 weeks of age. μCT-analyses showed that the 6-week-old female mice had increased femoral cortical thickness ($p < 0.001$) and decreased marrow volume ($p = 0.045$) (Fig. 5C), as well as decreased tibial trabecular thickness ($p = 0.044$) ($n = 7$–8/group) (Fig. 5D). Similar to the 6-week-old female mice, the 12-week-old female mice also had decreased tibial trabecular thickness ($p = 0.010$) and males had increased femoral cortical thickness ($p = 0.010$) ($n = 5$–6/group) (Fig. 5E). There were no significant differences in males at 6 weeks of age. In 26-week-old male mice, there were no changes in the trabecular bone, but a significant decrease in the cortical bone volume ($p = 0.003$) was found in the femurs ($n = 7$–8/group) (Fig. 5F). Taken together, deletion of Rcor2 in mesenchymal cell lineage caused no overt changes in bone quality, suggesting redundant function in regulation of bone homeostasis in normal healthy animals, possibly by a compensatory mechanism by other Rcor family members.

To study whether Rcor2 is required when bone turnover is accelerated, the bone parameters were studied in Rcor2$^{-/-}_{Prrx1}$ mice, which were challenged by OVX or by inducing a tibial fracture. In the OVX experiment, the bone mass of both control and Rcor2$^{-/-}_{Prrx1}$ animals was significantly reduced compared to sham-operated control animals. The conditional deletion of Rcor2 led to increased trabecular number in the OVX mice ($p = 0.028$), while the cortical bone analysis showed decreased cortical bone tissue volume ($p = 0.005$) and marrow volume ($p = 0.011$) ($n = 3$ sham/group, 7–8 OVX/group) (Fig. 6A). The analysis did not reveal other significant differences in the OVX response of conditional Rcor2 knockout. In the fracture experiment, Rcor2$^{-/-}_{Prrx1}$ mice were challenged by inducing a tibial fracture at 8 weeks of age. In the volumetric or mineral density analyses of the fracture callus, no differences in BMD, tissue volume or bone volume were found in the callus of the Rcor2$^{-/-}_{Prrx1}$ mice compared to controls in either males ($n = 5$–7/group) or females ($n = 8$–10/group) (Fig. 6B, C). The biomechanical analysis showed no significant changes in the stiffness, maximum load or post-yield displacement either, but the amount of work-to-fracture was significantly increased in the Rcor2$^{-/-}_{Prrx1}$ mice ($p < 0.001$, $n = 5$–7/group) (Fig. 6D-F).

3.5. *Rcor2 supports adipocyte differentiation in vitro and in vivo*

The increased expression of Rcor2 in differentiated adipocytes *in vitro* (Fig. 1D) raised the question whether downregulation of Rcor2 has an effect on adipose tissue *in vivo*. The fracture callus analysis revealed that the Rcor2$^{-/-}_{Prrx1}$ knockout mice had significantly less adipocytes inside the calluses compared to the controls ($p = 0.033$, $n = 8$/group) (Fig. 7A, B). There was also a significant decrease in the amount of inguinal adipose tissue in the Rcor2$^{-/-}_{Prrx1}$ mice compared to the controls at 16 weeks of age ($p = 0.034$, $n = 3$/group) (Fig. 7C). The capacity of primary cells extracted from the calvarias to differentiate into adipocytes (7 days) was also measured and there was a 45 % decrease in the area stained by Oil Red O *in vitro* in cultures derived from Rcor2KO$^{+/-}$

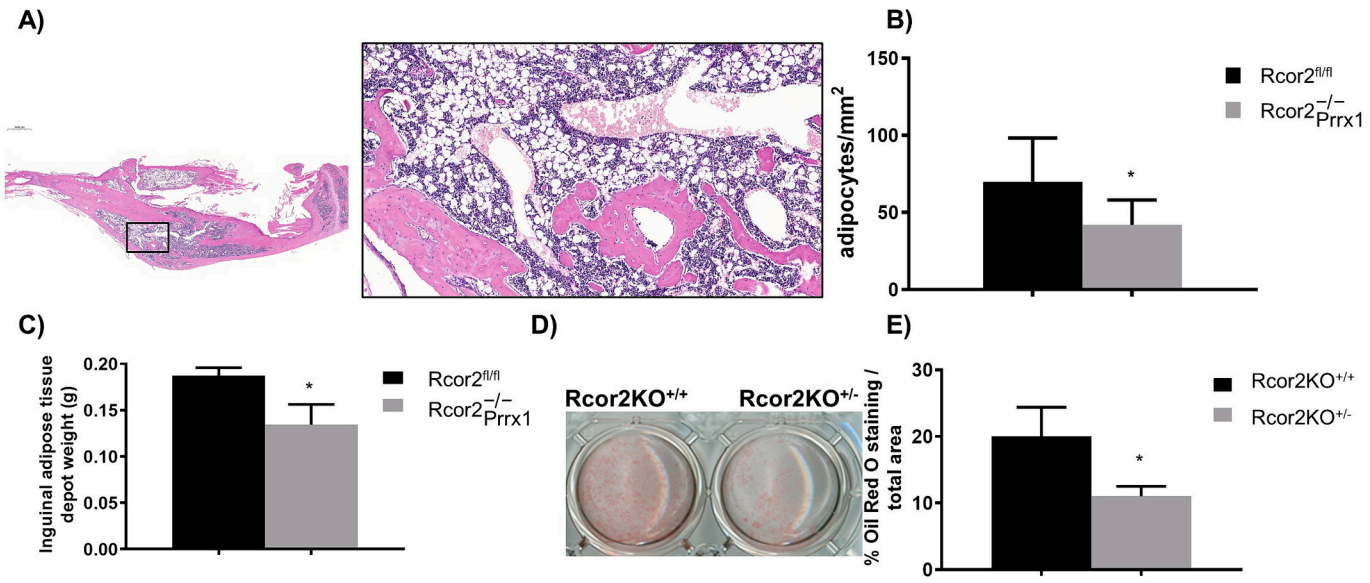

Fig. 7. Effect of Rcor2 on adipogenesis. A) Representative example of H&*E*-staining of fracture callus. B) The number of adipocytes calculated from a standardized area of $RCOR2_{Prrx1}$ mouse callus. KO mice ($n = 8$) had significantly less adipocytes than WT controls (n = 8). C) In $Rcor2^{-/-}_{Prrx1}$ mice (n = 3) inguinal white adipose tissue (WAT) mass was decreased compared to WT controls (n = 3). D) Oil Red O staining of $Rcor2^{+/-}$ mouse calvarial cells cultured in adipogenic differentiation media. E) $Rcor2^{+/-}$ calvarial cells formed significantly less differentiated adipocytes, as shown by area-based analysis of Oil Red O stained adipocytes. Cell culture data from a representative experiment of three independent experiments. Data are presented as means ± SD; *, $p < 0.05$. (For interpretation of the references to color in this figure legend, the reader is referred to the web version of this article.)

mice when compared to control mice ($p = 0.036$, $n = 3$/group) (Fig. 7D, E).

4. Discussion

In the present investigation, Rcor2 was identified as a significantly upregulated gene during the *in vitro* differentiation of osteoblasts and adipocytes and downregulation of Rcor2 mRNA expression was shown to lead to impaired differentiation of MC3T3-E1 cells and primary calvarial osteoblasts *in vitro*. The cells with lower Rcor2 expression were observed to respond to osteogenic stimulus with fewer transcriptional changes during the first 24 h of osteogenic stimulation, and they presented a distinguishable global gene expression profile compared to the control cells. However, targeted deletion of Rcor2 in mouse mesenchymal cells *in vivo* was dispensable for bone homeostasis, suggesting redundant roles for Rcor family members *in vivo*.

Functions of CoREST/Rcor family members have not been previously described in the MSC-derived cell lineages. However, Rcor proteins and especially Rcor1 have been implicated in regulating cell differentiation of neural and hematopoietic cell lineages [21,23,42–44], while the roles of Rcor2 and Rcor3 have so far been less studied. In the study of Yang and colleagues, knockdown of Rcor2 in embryonic stem cells (ESCs) led to proliferative defect and loss of pluripotency, and moreover, severely reduced iPS cell generation, indicating that Rcor2 is important in maintaining ESC pluripotency [45]. RNA-seq data presented in this investigation shows that downregulation of Rcor2 brought up GO terms such as chromatin and chromosome organization, as well as metabolic processes, suggesting a difference in the differentiation stage between ShScrambled and ShRCOR2–18 cells. Rcor2 has also been identified as a regulator of spermatogonial stem cell self-renewal and pluripotency [46], further supporting a significant role for Rcor2 in stem cell biology. However, abundant Rcor2 expression was found also in other tissues besides brain, testis and ESCs. Based on the current study, Rcor2 mRNA expression in MSCs at undifferentiated stage is low, unlike in ESCs or spermatogonial stem cells, while it becomes upregulated in the differentiated cells of adipocyte and osteogenic lineages. Thus, the finding that Rcor2 promotes osteoblast differentiation and is highly expressed in the late-stage osteoblasts, and in many other tissues as well, suggests that the function of Rcor2 is not restricted to stem cell stage, and its role in cell differentiation is probably complex and context-dependent.

Rcor2 is commonly found in complex with Lsd1, where it has been suggested to target the complex to demethylation sites of chromatin and Lsd1 to act as the functional complex member [39]. Lsd1 in turn has been demonstrated to play a role in several different MSC-related differentiation processes. Regarding osteoblast differentiation, Lsd1 activity was previously shown to inhibit osteogenic differentiation of human adipose-derived stem cells (hASCs), whereas Lsd1 inhibition promoted osteoblastogenesis [47]. This study found Rcor2 mRNA to be expressed broadly in adult mouse tissues but based on its expression level in whole transcriptome RNA-seq data, it clusters with the genes annotated to osteoblastic gene expression profile and is expressed predominantly in the bone cells of mesenchymal origin. Interestingly, Rcor proteins have recently been demonstrated to have also antagonistic actions in regulating Lsd1 activity at least in hematopoietic cells, suggesting that the coordinated regulation of Lsd1 by Rcors 1–3 is significant in regulating multilineage differentiation [23]. Although Rcor1 and Rcor3 are also expressed in osteoblasts, these data indicate that Rcor2 is the most dynamically regulated during differentiation. However, the presence of all Rcor family members in a cell may allow the formation of multiple complexes with Lsd1, the potentially differential roles of these complexes remain to be clarified. Lsd1 is known to promote normal hematopoietic differentiation but promote dedifferentiation during leukemogenesis [48], highlighting again the importance of recognition of mechanisms of Lsd1-Rcor complex in different cellular contexts.

Interestingly, significant enrichment of DE genes in pathways related to cellular energy metabolism, including amino acid, fatty acid, and cholesterol synthesis and catabolism, was found in the Rcor2 knockdown experiment in osteoblastic MC3T3-E1 cells. The findings of lower inguinal white adipose tissue mass and decreased adipocyte number in the fracture calluses suggest that Rcor2 might have a role in regulating the actions of Lsd1 in cellular energy metabolism also in other cell types, such as adipocytes [49]. However, this investigation did not address the expression of adipokines, white adipose tissue in other depots nor brown adipose tissue, leaving space for further studies to elucidate the

phenotype in more detail.

In conclusion, these results suggest that Rcor2 mediates the epigenetic regulation of gene transcription and has a significant role in regulating MSC commitment and differentiation to adipocyte and osteoblast lineages, at least *in vitro*. However, several questions remain open regarding the actions of Rcor2. While Rcor2 alone did not control osteoblast differentiation *in vivo*, these results pave the way for better understanding of co-regulatory activity on epigenetic factors.

Supplementary data to this article can be found online at https://doi.org/10.1016/j.bone.2024.117180.

Funding

This study was funded by the Academy of Finland (R.K.: 298625, 268535, 139165).

CRediT authorship contribution statement

Petri Rummukainen: Writing – review & editing, Writing – original draft, Visualization, Methodology, Investigation, Formal analysis. **Kati Tarkkonen:** Writing – original draft, Visualization, Supervision, Methodology, Investigation, Funding acquisition, Formal analysis, Conceptualization. **Rana Al Majidi:** Writing – original draft, Visualization, Investigation, Formal analysis. **Tero Puolakkainen:** Writing – original draft, Investigation, Formal analysis. **Vappu Nieminen-Pihala:** Writing – original draft, Visualization, Investigation, Formal analysis. **Cristina Valensisi:** Writing – original draft, Investigation, Formal analysis, Data curation. **Lauri Saastamoinen:** Writing – original draft, Visualization, Investigation, Formal analysis. **David Hawkins:** Investigation, Data curation. **Terhi J. Heino:** Writing – original draft, Supervision. **Kaisa K. Ivaska:** Writing – original draft, Supervision. **Riku Kiviranta:** Writing – original draft, Supervision, Resources, Funding acquisition, Conceptualization.

Declaration of competing interest

None.

Data availability

Data will be made available on request.

Acknowledgements

The authors thank Merja Lakkisto, Dr. Fan Wang, Turku Center for Disease Modeling (TCDM) and the staff of Turku Central Animal Laboratory for their excellent technical assistance.

References

[1] L. Oton-Gonzalez, C. Mazziotta, M.R. Iaquinta, E. Mazzoni, R. Nocini, L. Trevisiol, A. D'Agostino, et al., Genetics and epigenetics of bone remodeling and metabolic bone diseases, Int. J. Mol. Sci. [Internet]. 23 (3) (2022 Jan 28) 1500. Available from: https://pubmed.ncbi.nlm.nih.gov/35163424.

[2] H.W. Lee, J.H. Suh, A.Y. Kim, Y.S. Lee, S.Y. Park, J.B. Kim, Histone deacetylase 1-mediated histone modification regulates osteoblast differentiation, Mol. Endocrinol. 20 (10) (Oct 1 2006) 432–443 [Internet].. Available from, https://doi.org/10.1210/me.2006-0061.

[3] Paino F, La Noce M, Tirino V, Naddeo P, Desiderio V, Pirozzi G, De Rosa A, et al. Histone deacetylase inhibition with valproic acid downregulates osteocalcin gene expression in human dental pulp stem cells and osteoblasts: evidence for HDAC2 involvement. Stem Cells Int. 2014 Jan;32(1):279–89. Available from: https://pubmed.ncbi.nlm.nih.gov/24105979.

[4] Razidlo DF, Whitney TJ, Casper ME, McGee-Lawrence ME, Stensgard BA, Li X, Secreto FJ, et al. Histone deacetylase 3 depletion in osteo/chondroprogenitor cells decreases bone density and increases marrow fat. PLoS One [Internet]. 2010 Jul 9; 5(7):e11492–e11492. Available from: https://pubmed.ncbi.nlm.nih.gov/20628553.

[5] J.S. Kang, T. Alliston, R. Delston, R. Derynck, Repression of Runx2 function by TGF-beta through recruitment of class II histone deacetylases by Smad3, EMBO J [Internet]. 24 (14) (2005/06/30), 2005 Jul 20. 2543–55. Available from: https://pubmed.ncbi.nlm.nih.gov/15990875.

[6] Dudakovic A, Gluscevic M, Paradise CR, Dudakovic H, Khani F, Thaler R, Ahmed FS, et al. Profiling of human epigenetic regulators using a semi-automated real-time qPCR platform validated by next generation sequencing. Gene. 2017/01/27. 2017 Apr;609:28–37.

[7] J.J. Westendorf, S.K. Zaidi, J.E. Cascino, R. Kahler, A.J. van Wijnen, J.B. Lian, M. Yoshida, et al., Runx2 (Cbfa1, AML-3) Interacts with Histone Deacetylase 6 and Represses the p21<sup>CIP1/WAF1</sup&gt, Promoter. Mol. Cell. Biol. [Internet] 22 (22) (2002 Nov 15), 7982 LP – 7992. Available from: http://mcb.asm.org/content/22/22/7982.abstract.

[8] Jensen ED, Schroeder TM, Bailey J, Gopalakrishnan R, Westendorf JJ. Histone deacetylase 7 associates with Runx2 and represses its activity during osteoblast maturation in a deacetylation-independent manner. J Bone Miner Res [Internet]. 2008 Mar;23(3):361–72. Available from: https://pubmed.ncbi.nlm.nih.gov/17997710.

[9] M. Haberland, M.H. Mokalled, R.L. Montgomery, E.N. Olson, Epigenetic control of skull morphogenesis by histone deacetylase 8, Genes Dev. 23 (14) (2009 Jul) 1625–1630.

[10] M.M. Musri, M.C. Carmona, F.A. Hanzu, P. Kaliman, R. Gomis, M. Parrizas, Histone demethylase LSD1 regulates adipogenesis, J. Biol. Chem. 285 (39) (Sep 2010) 30034–30041.

[11] M. Yang, C.B. Gocke, X. Luo, D. Borek, D.R. Tomchick, M. Machius, Z. Otwinowski, et al., Structural basis for CoREST-dependent demethylation of nucleosomes by the human LSD1 histone demethylase, Mol. Cell 23 (3) (Aug 2006) 377–387.

[12] G.I. Nic-Can, B.A. Rodas-Junco, L.M. Carrillo-Cocom, A. Zepeda-Pedreguera, R. Peñaloza-Cuevas, F.J. Aguilar-Ayala, R.A. Rojas-Herrera, Epigenetic regulation of Adipogenic differentiation by histone lysine demethylation, Int. J. Mol. Sci. [Internet]. 20 (16) (2019 Aug 12) 3918. Available from: https://pubmed.ncbi.nlm.nih.gov/31408999.

[13] D. Yang, H. Okamura, Y. Nakashima, T. Haneji, Histone demethylase Jmjd3 regulates osteoblast differentiation via transcription factors Runx2 and osterix, J. Biol. Chem. 288 (47) (Nov 2013) 33530–33541.

[14] L. Ye, Z. Fan, B. Yu, J. Chang, K. Al Hezaimi, X. Zhou, N.-H. Park, et al., Histone demethylases KDM4B and KDM6B promotes osteogenic differentiation of human MSCs, Cell Stem Cell 11 (1) (July 2012) 50–61.

[15] K.M. Sinha, H. Yasuda, X. Zhou, B. deCrombrugghe, Osterix and NO66 histone demethylase control the chromatin of Osterix target genes during osteoblast differentiation, J. Bone Miner. Res. 29 (4) (Apr 2014) 855–865.

[16] P. Rummukainen, K. Tarkkonen, A. Dudakovic, R. Al-Majidi, V. Nieminen-Pihala, C. Valensisi, R.D. Hawkins, et al., Lysine-Specific Demethylase 1 (LSD1) epigenetically controls osteoblast differentiation, PLoS One [Internet] 17 (3) (2022 Mar 7) e0265027. Available from, https://doi.org/10.1371/journal.pone.0265027.

[17] E. Metzger, M. Wissmann, N. Yin, J.M. Muller, R. Schneider, A.H. Peters, T. Gunther, et al., LSD1 demethylates repressive histone marks to promote androgen-receptor-dependent transcription, Nature 437 (7057) (2005 Sep) 436–439.

[18] C. Cai, H.H. He, S. Chen, I. Coleman, H. Wang, Z. Fang, S. Chen, et al., Androgen receptor gene expression in prostate cancer is directly suppressed by the androgen receptor through recruitment of lysine-specific demethylase 1, Cancer Cell 20 (4) (Oct 2011) 457–471.

[19] I. Garcia-Bassets, Y.S. Kwon, F. Telese, G.G. Prefontaine, K.R. Hutt, C.S. Cheng, B. G. Ju, et al., Histone methylation-dependent mechanisms impose ligand dependency for gene activation by nuclear receptors, Cell 128 (3) (2007 Feb) 505–518.

[20] E.A. Clark, F. Wu, Y. Chen, P. Kang, U.B. Kaiser, R. Fang, Y.G. Shi, GR and LSD1/KDM1A-targeted gene activation requires selective H3K4me2 demethylation at enhancers, Cell Rep. 27 (12) (Jun 18 2019) 3522–3532.e3 [Internet].. Available from, https://doi.org/10.1016/j.celrep.2019.05.062.

[21] C.I. Lopez, K.E. Saud, R. Aguilar, F.A. Berndt, J. Cánovas, M. Montecino, M. Kukuljan, The chromatin modifying complex CoREST/LSD1 negatively regulates notch pathway during cerebral cortex development, Dev. Neurobiol. 76 (12) (2016 Dec), 1360–73.

[22] X. Hu, X. Li, K. Valverde, X. Fu, C. Noguchi, Y. Qiu, S. Huang, LSD1-mediated epigenetic modification is required for TAL1 function and hematopoiesis, Proc. Natl. Acad. Sci. USA 106 (25) (Jun 2009) 10141–10146.

[23] G. Upadhyay, A.H. Chowdhury, B. Vaidyanathan, D. Kim, S. Saleque, Antagonistic actions of Rcor proteins regulate LSD1 activity and cellular differentiation, Proc Natl Acad Sci 111 (22) (2014) 8071–8076 [Internet].. Available from:http://www.pnas.org/cgi/, https://doi.org/10.1073/pnas.1404292111.

[24] Y.J. Shi, C. Matson, F. Lan, S. Iwase, T. Baba, Y. Shi, Regulation of LSD1 histone demethylase activity by its associated factors, Mol. Cell 19 (6) (2005 Sep), 857–64.

[25] Nieminen-Pihala V, Tarkkonen K, Laine J, Rummukainen P, Saastamoinen L, Nagano K, Baron R, et al. Early B-cell Factor1 (Ebf1) promotes early osteoblast differentiation but suppresses osteoblast function. Bone [Internet]. 2021;146: 115884. Available from: https://www.sciencedirect.com/science/article/pii/S8756328221000466.

[26] F. Wang, K. Tarkkonen, V. Nieminen-Pihala, K. Nagano, Majidi R. Al, T. Puolakkainen, P. Rummukainen, et al., Mesenchymal cell-derived Juxtacrine Wnt1 signaling regulates osteoblast activity and osteoclast differentiation, J. Bone Miner. Res. 34 (6) (Jun 1 2019) 1129–1142 [Internet].. Available from: https://doi.org/10.1002/jbmr.3680.

[27] M.S. Lehti, H. Henriksson, P. Rummukainen, F. Wang, L. Uusitalo-Kylmälä, R. Kiviranta, T.J. Heino, et al., Cilia-related protein SPEF2 regulates osteoblast

differentiation, Sci. Rep. [Internet]. 8 (1) (2018 Jan 16) 859. Available from: https://pubmed.ncbi.nlm.nih.gov/29339787.
[28] A. Dudakovic, E. Camilleri, S.M. Riester, E.A. Lewallen, S. Kvasha, X. Chen, D. J. Radel, et al., High-resolution molecular validation of self-renewal and spontaneous differentiation in clinical-grade adipose-tissue derived human mesenchymal stem cells, J. Cell. Biochem. 115 (10) (2014 Oct), 1816–28.
[29] D. Kim, G. Pertea, C. Trapnell, H. Pimentel, R. Kelley, S.L. Salzberg, TopHat2: accurate alignment of transcriptomes in the presence of insertions, deletions and gene fusions, Genome Biol. [Internet]. 14 (4) (2013) R36. Available from: https://doi.org/10.1186/gb-2013-14-4-r36.
[30] S. Anders, W. Huber, Differential expression analysis for sequence count data, Genome Biol. [Internet]. 11 (10) (2010) R106. Available from: https://doi.org/10.1186/gb-2010-11-10-r106.
[31] Y. Benjamini, Y. Hochberg, Controlling the false discovery rate: a practical and powerful approach to multiple testing, J R Stat Soc Ser B [Internet]. 57 (1) (1995 Jan 1) 289–300. Available from: https://doi.org/10.1111/j.2517-6161.1995.tb02031.x.
[32] T. Giorgino, Computing and Visualizing Dynamic Time Warping Alignments in R: The dtw Package, J. Stat. Softw. 1 (7) (2009). Vol. Issue. [Internet]. Available from: https://www.jstatsoft.org/v031/i07.
[33] Sakai K, Miyazaki J. A transgenic mouse line that retains Cre recombinase activity in mature oocytes irrespective of thecreTransgene transmission. Biochem. Biophys. Res. Commun. [Internet]. 1997;237(2):318–24. Available from: https://www.sciencedirect.com/science/article/pii/S0006291X97971114.
[34] T. Biosciences, Flp Deleter [Internet], Available from, https://www.taconic.com/mouse-model/flp-deleter.
[35] T. Puolakkainen, P. Rummukainen, J. Lehto, O. Ritvos, A. Hiltunen, A.-M. Saamanen, R. Kiviranta, Soluble activin type IIB receptor improves fracture healing in a closed tibial fracture mouse model, PLoS One 12 (7) (2017) e0180593.
[36] A. Hiltunen, E. Vuorio, H.T. Aro, A standardized experimental fracture in the mouse tibia, J. Orthop. Res. Off. Publ. Orthop. Res. Soc. 11 (2) (1993 Mar), 305–12.
[37] Heydarpour P, Salehi-Sadaghiani M, Javadi-Paydar M, Rahimian R, Fakhfouri G, Khosravi M, Khoshkish S, et al. Estradiol reduces depressive-like behavior through inhibiting nitric oxide/cyclic GMP pathway in ovariectomized mice. Horm. Behav. [Internet]. 2013;63(2):361–9. Available from: https://www.sciencedirect.com/science/article/pii/S0018506X12003029.
[38] D.W. Dempster, J.E. Compston, M.K. Drezner, F.H. Glorieux, J.A. Kanis, H. Malluche, P.J. Meunier, et al., Standardized nomenclature, symbols, and units for bone histomorphometry: a 2012 update of the report of the ASBMR Histomorphometry nomenclature committee, J. Bone Miner. Res. 28 (1) (2013) 2–17.
[39] Y. Wang, Q. Wu, P. Yang, C. Wang, J. Liu, W. Ding, W. Liu, et al., LSD1 co-repressor Rcor2 orchestrates neurogenesis in the developing mouse brain, Nat. Commun. 7 (2016 Jan) 10481.
[40] X. Hu, W.-P. Li, C. Meng, L.B. Ivashkiv, Inhibition of IFN-gamma signaling by glucocorticoids, J. Immunol. 170 (9) (2003 May), 4833–9.
[41] C.E. Monaghan, T. Nechiporuk, S. Jeng, S.K. McWeeney, J. Wang, M.G. Rosenfeld, G. Mandel, REST corepressors RCOR1 and RCOR2 and the repressor INSM1 regulate the proliferation-differentiation balance in the developing brain, Proc. Natl. Acad. Sci. USA 114 (3) (2017 Jan). E406–15.
[42] Andrés ME, Burger C, Peral-Rubio MJ, Battaglioli E, Anderson ME, Grimes J, Dallman J, et al. CoREST: a functional corepressor required for regulation of neural-specific gene expression. Proc Natl Acad Sci [Internet]. 1999;96(17):9873–8. Available from: http://www.pnas.org/content/96/17/9873.abstract.
[43] Fuentes P, Canovas J, Berndt FA, Noctor SC, Kukuljan M. CoREST/LSD1 control the development of pyramidal cortical neurons. Cereb cortex (New York, NY 1991). 2012 Jun;vol. 22(6):1431–41.
[44] S. Saleque, J. Kim, H.M. Rooke, S.H. Orkin, Epigenetic regulation of hematopoietic differentiation by Gfi-1 and Gfi-1b is mediated by the cofactors CoREST and LSD1, Mol. Cell 27 (4) (2007 Aug), 562–72.
[45] P. Yang, Y. Wang, J. Chen, H. Li, L. Kang, Y. Zhang, S. Chen, et al., RCOR2 is a subunit of the LSD1 complex that regulates ESC property and substitutes for SOX2 in reprogramming somatic cells to pluripotency, Stem Cells 29 (5) (2011 May) 791–801.
[46] Q. Zhou, Y. Guo, B. Zheng, B. Shao, M. Jiang, G. Wang, T. Zhou, et al., Establishment of a proteome profile and identification of molecular markers for mouse spermatogonial stem cells, J. Cell. Mol. Med. 19 (3) (2015 Mar) 521–534.
[47] Ge W, Liu Y, Chen T, Zhang X, Lv L, Jin C, Jiang Y, et al. The epigenetic promotion of osteogenic differentiation of human adipose-derived stem cells by the genetic and chemical blockade of histone demethylase LSD1. Biomaterials. [Internet]. 2014;35(23):6015–25. Available from: http://www.sciencedirect.com/science/article/pii/S0142961214004530.
[48] A. Maiques-Diaz, G.J. Spencer, J.T. Lynch, F. Ciceri, E.L. Williams, F.M.R. Amaral, D.H. Wiseman, et al., Enhancer activation by pharmacologic displacement of LSD1 from GFI1 induces differentiation in acute myeloid leukemia, Cell Rep. 22 (13) (2018 Mar), 3641–59.
[49] F.A. Hanzu, M.M. Musri, A. Sánchez-Herrero, M. Claret, Y. Esteban, P. Kaliman, R. Gomis, et al., Histone demethylase KDM1A represses inflammatory gene expression in preadipocytes, Obesity (Silver Spring) 21 (12) (2013 Dec). E616–25.